Optimal Design of Grating-Assisted Directional Couplers

Vittorio M. N. Passaro, *Member, IEEE*

***Abstract*—In this paper, a rigorous leaky mode propagation method has been used to investigate the influence of the grating period and grating index profile on the design of grating-assisted directional couplers (GADC's). A detailed explanation of resonance condition and radiation loss in terms of electromagnetic field contribution in the grating region as a function of the grating period and profile is given. Optimal design parameters have been found for well-defined structures in order to achieve either minimum coupling length or maximum coupling efficiency. A very fast method to extract the resonance condition in any grating-assisted structure by using a sinusoidal profile is proposed. Numerical results are presented for both moderately and strongly asymmetric structures in terms of normalized propagation constant, mode radiation loss, coupling length and coupling efficiency. Comparisons with grating period and coupling length predictions obtained by other methods are also shown. The rectangular profile with optimized duty cycle has been demonstrated to be the best choice in order to minimize the GADC coupling length.**

***Index Terms*—Gratings, optical directional couplers.**

I. Introduction

A NUMBER of methods have been proposed in literature for the analysis and design of grating-assisted directional couplers (GADC's), which are fundamental guided-wave components for many applications including contradirectional coupling [1], distributed Bragg reflector sources [2], optical wavelength filtering [3], [4], wavelength-division multiplexing (WDM) [5].

The coupled-mode theory (CMT) has been used for describing the power transfer between the two waveguides of a GADC in terms of ideal waveguide composite modes [6], [7]. An approximated CMT method has been proposed in [8] to calculate the radiation loss. Several higher order perturbation methods, derived by CMT approach, have been used to predict a number of secondary effects occurring in the GADC structure [9]–[11]. A different approach is the transfer matrix method (TMM) [12], which allows simple calculations of the GADC design parameters, such as grating period and coupling length, as well as approximated calculations of the scattering loss induced at the grating transverse interfaces. The approximations included by both CMT and TMM methods increase with increasing the grating depth and GADC asymmetry. The Floquet theory, first introduced by Chang *et al.* [13], allows rigorous analysis of grating out-couplers. It has been also used to analyze the radiation loss in GADC in terms of leaky mode propagation (LMP) [14]. The method is based on the expansion of the composite modes of the structure in an infinite number of space harmonics due to the presence of the grating. The power carried by each harmonic is partially guided along the propagation direction and partially radiated in the external semi-infinite regions. The power exchange between each pair of space harmonics is governed by the Floquet theorem. Recently, the Floquet–Bloch theory has been utilized to determine the optimal grating period (resonance condition) and other GADC properties [15], and to design the semiconductor-glass composed directional couplers [16] and metallized-grating GADC's [17]. However, a complete investigation of the influence of grating index profile on the GADC performance has not yet been considered. The aim of this paper is the analysis of both moderately and strongly asymmetric GADC's as a function of the index profile. Since the LMP approach does not introduce any theoretical approximation, it represents a powerful method to understand how critical is the influence of the grating period and profile on all the GADC parameters. Moreover, it allows the accurate calculation of all the design parameters, including power coupling length, coupling efficiency, power attenuation coefficient and total radiation loss. Thus, the geometrical characteristics of GADC's, optimized with respect to different constraints, such as minimum coupling length or maximum coupling efficiency, can be found (optimal design).

In Section II the theoretical analysis of a GADC structure having arbitrary grating profile is presented. In Section III numerical results are presented for the analysis of a InP–In_xGa_{1-x}AsP–InP–In_yGa_{1-y}AsP–InP GADC structure working at the free-space optical wavelength $\lambda_o = 1.5\ \mu$m with TE polarization. A detailed explanation of resonance condition and mode radiation loss is given. Comparisons of our method with CMT and TMM are performed in terms of grating period, power coupling length and efficiency for GADC's having moderate asymmetry. Section IV summarizes the conclusions.

II. Analysis of the GADC Structure

The schematic diagram of the GADC structure is shown in Fig. 1. A periodic perturbation, having period Λ and length L and arbitrary index profile, is placed on the lower waveguide, being x the depth and z the length direction. Each layer of the structure is assumed isotropic, homogeneous, lossless and two-dimensional. The scalar wave equation is given by

$$d^2F_i(x,z)/dx^2 + d^2F_i(x,z)/dz^2 + k_o^2\epsilon_i(x,z)F_i(x,z) = 0 \quad (1)$$

Manuscript received October 22, 1999; revised February 23, 2000.

The author is with the Optoelectronics Laboratory, Dipartimento di Elettrotecnica ed Elettronica, Politecnico di Bari, 4-70125 Bari, Italy.

Publisher Item Identifier S 0733-8724(00)05761-3.

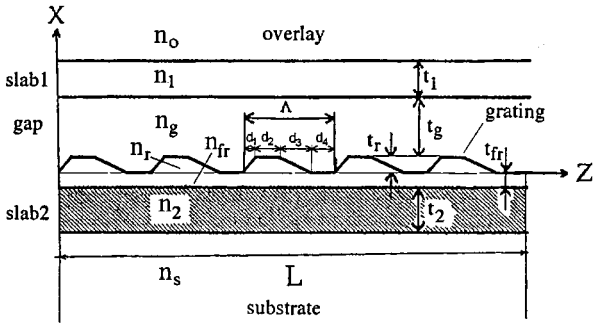

Fig. 1. Schematic diagram of the GADC structure with arbitrary profile. GADC parameters: overlay n_o, upper slab n_1, gap n_g, grating n_r, underlayer n_{fr}, lower slab n_2, substrate n_s refraction indices, and upper slab t_1, gap t_g, grating $t_r = t$, underlayer t_{fr}, lower slab t_2 thicknesses. d_1, d_2, d_3, d_4 are the profile parameters, Λ the grating period and L the grating length.

where F_i is the appropriate electric or magnetic field y-component (i.e., $F_i = E_y$ for transverse electric (TE) and $F_i = H_y$ for transverse magnetic (TM) polarization), k_o is the free-space wavenumber, i designates the generic homogeneous layer, $i = o, 1, g, r, fr, 2, s$, and $\epsilon_i(x, z)$ is the relevant permittivity. The permittivity function is periodical along z only in the grating region, i.e., $\epsilon_r(x, z)$, and it can be written according to the Fourier series expansion as

$$\epsilon_r(x,z) = \sum_n \epsilon_n(x) \exp(j2\pi nz/\Lambda) \tag{2}$$

where n denotes the nth space harmonic, and

$$\epsilon_n(x) = (1/\Lambda) \int_{-\Lambda/2}^{+\Lambda/2} \epsilon(x,z) \exp(-j2\pi nz/\Lambda)\, dz \tag{3}$$

is the nth series coefficient. Thus, the solution of (1) in the grating region, according to the Floquet space harmonics expansion [13], [14], is

$$F_r(x,z) = \sum_n f_n(x) \exp(jk_{zn}z) \qquad 0 \le x \le t_r \tag{4}$$

where $f_n(x)$ is the nth space harmonic amplitude function and k_{zn} is the component along z of the relevant propagation vector. It is well known that the nth component is related to the fundamental harmonic $(n = 0)$ by the Floquet phase relationship [13], i.e., $k_{zn} = k_{z0} + 2\pi n/\Lambda$, where k_{z0} refers to the zeroth-order mode of the perturbed structure. Therefore, the field in the grating region assumes the form of a superposition of space harmonics. In order to completely describe the electromagnetic field in the GADC structure, we denote *as* the z-component of the e.m. field ($G_i = H_z$ for TE and $G_i = E_z$ for TM polarization, respectively). Similarly to (4), it results in the grating region

$$G_r(x,z) = \sum_n g_n(x) \exp(jk_{zn}z) \qquad 0 \le x \le t_r \tag{5}$$

where $g_n(x)$ is the relevant nth hsrmonic amplitude function. Moreover, the relationships between the $f_n(x)$ and $g_n(x)$ field component amplitudes have been determined by using the Maxwell equations

$$\begin{aligned} df_n(x)/dx &= \sum_l q_{nl} g_l(x) \\ dg_n(x)/dx &= \sum_n p_{nm} f_m(x) \end{aligned} \tag{6}$$

where q_{nl} and p_{nm} are elements of two squared matrices, each one depending on the permittivity coefficients. In case of TE polarization, we have

$$\begin{aligned} g_{nl}(x) &= -j\omega\mu_0\delta_{nl} \\ p_{nm}(x) &= j\omega\epsilon_0[(k_{zn}/k_o)^2\delta_{nm} - \epsilon_{m-n}(x)] \end{aligned} \tag{7}$$

being δ_{nm}, δ_{nl} Kronecker's delta functions, and $\epsilon_{m-n}(x)$ the appropriate coefficient of Floquet series expansion. The solution of (6), together with the continuity conditions applied to each longitudinal interface between different layers, allows to find the propagation constants and the field distributions of all the field space harmonics retained in the analysis. In particular, the continuity conditions can be summarized for TE-polarized mode [14] as

$$df_n(0)/dx + j[1 - r_n^{(fr)}]/[1 + r_n^{(fr)}]k_{xn}^{(fr)} f_n(0) = 0 \tag{8}$$

$$\begin{aligned} df_n(t_r)/dx - jk_{xn}^{(g)} f_n(t_r)[1 - r_n^{(g)} \exp(j2k_{xn}^{(g)} t_r)]/ \\ [1 + r_n^{(g)} \exp(j2k_{xn}^{(g)} t_r)] = 0 \end{aligned} \tag{9}$$

where $x = t_r = t$ is the grating thickness, $k_{xn}^{(fr)}$, $k_{xn}^{(g)}$ are the nth harmonic x-components of the wave vector in the layers fr and g, respectively, and the coefficients $r_n^{(fr)}$, $r_n^{(g)}$ depend on the propagation constant components in the same layers. It must be noted that the condition (7) includes a dependence of the solutions in the grating region on the equivalent permittivity

$$\epsilon_{\rm eq}(x) = (k_{zn}/k_o)^2\delta_{nm} - \epsilon_{m-n}(x)$$

which is a function of both the space harmonic order n and the grating profile. This has important consequences, as it will be better clarified in the following. From the equation system (6) it is clear that an arbitrary but finite number of harmonics, say $2N + 1$, has to be taken for numerical integration, having the complex wave-number $k_{zo} = \beta_o + j\alpha$ of the GADC composite guided mode as unknown variable, where $\alpha > 0$ is the mode amplitude attenuation coefficient (leakage factor). In other words, the LMP approach explains the radiating effect produced by the grating in terms of leaky modes, having field space harmonics which radiate power in the semi-infinite regions. In order to numerically integrate the system (6), a four-order Runge–Kutta algorithm has been used, which gives accurate results also for large grating depths when a large enough number of iterations is used (up to 50 iterations have been used for $t < 0.15$ μm). Moreover, the complex eigenvalue k_{zo} has been found by the Muller's method. After finding k_{zo}, the amplitude coefficients of each space harmonic and k_{zn}, $k_{xn}^{(i)}$, $f_n(0)$, $f_n(t_r)$ have been determined. Details of numerical procedure can be found in [14]. Strong attention must be paid to the choice of the starting point, i.e., the approximated propagation constant, in order to avoid double roots. The problem is well described in [15].

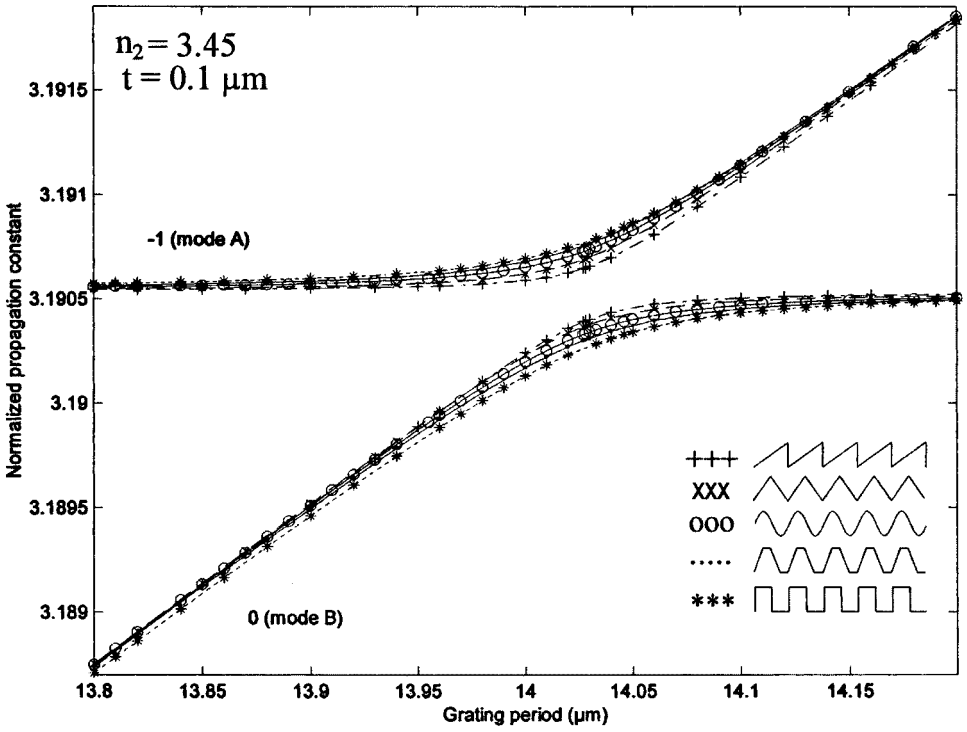

Fig. 2. Real part of normalized propagation constant of $n = -1$ (mode A) and $n = 0$ (mode B) space harmonics versus grating period for different index profiles, +++: sawtooth, $\times\times\times$: symmetric triangular, ooo: sinusoidal, . . .: symmetric trapezoidal, ***: squared (50%). GADC parameters: $n_o = 3.18$, $n_1 = 3.282$, $n_g = 3.18$, $n_r = n_{fr} = 3.282$, $n_2 = 3.45$, $n_s = 3.18$, $t_1 = 0.2$ μm, $t_r = 0.1$ μm, $t_g = 1.45$ μm, $t_{fr} = 0.45$ μm, $t_2 = 0.257$ μm.

III. Numerical Results

A. Grating Resonance Condition

The GADC structure already presented by Marcuse [8] and considered by Sun *et al.* [15] has been largely investigated. It consists in a InP–$In_xGa_{1-x}AsP$–InP–$In_xGa_{1-x}AsP$–$In_yGa_{1-y}AsP$–InP multilayered structure, having parameters $n_o = 3.18$, $n_1 = 3.282$, $n_g = 3.18$, $n_{fr} = 3.282$, $n_s = 3.18$, $t_1 = 0.2$ μm, and $t_g + t_r + t_{fr} = 2$ μm. The monomodal condition [8] $2t_2\sqrt{n_2^2 - 3.18^2} + 0.8119 = \lambda_o$ allows to obtain t_2 as a function of n_2, being λ_o the free-space optical wavelength. The choice to have only two ideal composite modes is similar to the TMM approach, in which only two local normal modes are considered at each grating section [12]. As a first step, we have calculated the composite modes of the same structure as above, but unperturbed ($t_g = 1.5$ μm, $t_r = 0$, $t_{fr} = 0.5$ μm, $n_2 = 3.45$, $t_2 = 0.257$ μm) at $\lambda_o = 1.5$ μm. Results give $n_{\text{eff}}^A \sim 3.2974545$ and $n_{\text{eff}}^B \sim 3.1906012$, being mode A (even) mainly confined in the lower slab and B (odd) in the upper one. Then, a similar structure with a grating depth of $t_r = t = 0.1$ μm ($t_g = 1.45$ μm, $t_{fr} = 0.45$ μm) has been investigated. It is well known that the grating period, needed to have a high-efficiency power transfer between the ideal composite modes of the structure, depends on the effective index difference between the two guided modes exchanging power along z. The conventional CMT method determines the grating period in an approximated form

$$\Lambda = \lambda_o/[n_{\text{eff}}^{(\text{even})} - n_{\text{eff}}^{(\text{odd})}] = 14.038\ \mu\text{m}. \tag{10}$$

The TMM approach [12] gives in this case (strongly asymmetric) a much more approximated value of the grating period

$$\Lambda = \Lambda^- + \Lambda^+ = \lambda_o/[n_{\text{eff}}^{(1,\text{inf})} - n_{\text{eff}}^{(2,\text{inf})}] + \lambda_o/[n_{\text{eff}}^{(1,\text{supp})} - n_{\text{eff}}^{(2,\text{sup})}] = 40.258\ \mu\text{m} \tag{11}$$

being "inf" and "sup" the local sections of the grating period. In the LMP approach, the optimal grating period is found at the resonance condition [15], i.e., when the deviation $\delta = \beta_0^A - \beta_0^B - K$ from the exact synchronization condition between the modes A and B, i.e., $\beta_0^B = \beta_0^A - K$, is minimized, being K the grating wavevector and β_0^A, β_0^B the real parts of the fundamental (zeroth-order) harmonic propagation constants of mode A and B, respectively. Since $\beta_{-1}^A = \beta_0^A - K$, where β_{-1}^A is the real part of -1 harmonic propagation constant of mode A, the resonance condition implies also that the EM-field distribution of -1 harmonic of mode A is more similar to that of 0 harmonic of mode B or, in other words, the difference of their phase velocities is minimal. The resulting coupling length, allowing the maximum power transfer between the lower and upper slabs, is given by the well-known formulation [15], [16]

$$L_c = \frac{\pi}{\delta} \tag{12}$$

which is used in the CMT approach, too [6], [18].

Fig. 2 shows the effective indices of -1 (mode A) and 0 (mode B) space harmonic as a function of the grating period. A number of different index profiles have been considered: sawtooth (+++, with $d_1 = \Lambda$, $d_2 = d_3 = d_4 = 0$), symmetric triangular ($\times\times\times$, $d_1 = \Lambda/2$, $d_2 = d_4 = 0$, $d + 3 = \Lambda/2$),

sinusoidal (ooo), symmetric trapezoidal ($\cdots, d_1 = d_2 = d_3 = d_4 = \Lambda/4$), rectangular profile with a 50% duty cycle (***, $d_1 = d_3 = 0$, $d_2 = d_4 = \Lambda/2$). The meaning of d_i parameters is illustrated in Fig. 1. From Fig. 2, it can be clearly seen that the resonance condition occurs when δ is minimal. The calculations highlight a little change of resonant period for each profile, being $\Lambda = 14.029$ μm for sinusoidal, trapezoidal and triangular, 14.031 μm for sawtooth, and 14.033 μm for rectangular profile, respectively. However, the change is very moderate, so demonstrating that the grating period which matches to the best the field distributions of perturbed structure modes depends very slightly on the index profile, even for strongly asymmetric GADC (in this case $t = 0.1$ μm).

For instance, the presence of the grating in the GADC structure causes three fundamental effects. The first is that each guided mode generates infinite space harmonics (with $n < -1$ for mode A and $n < 0$ for mode B), radiating power in the substrate and in the overlay. The second is that only two space harmonics ("fundamental") carry significant guided power in the upper and lower slabs (with $n = -1$ and $n = 0$ for mode A and $n = 0, n = 1$ for mode B). The third effect implies that the e.m. fields of space harmonics having $\epsilon_{\rm eq}(x) > 0$ are confined in the grating region (hereinafter "spurious" harmonics). This circumstance occurs for the harmonics having $n > 0$ (mode A) or $n > 1$ (mode B) for the structures considered in this paper. These confinements depends on the permittivity coefficients of the Fourier series expansion (3) of the grating profile, which are contained in $\epsilon_{\rm eq}(x)$, and cause a distorsion of e.m. field distribution of fundamental harmonics from "ideal" condition in absence of grating, i.e., $\delta = 0$. As a consequence, at the resonance the influence of spurious harmonics is minimal since their amplitudes, depending on the equivalent permittivity, are globally minimized.

The amplitudes of spurious harmonics have been calculated at the resonance and near the resonance for different profiles (D = sawtooth, S = sinusoidal, T = triangular, Q = squared, TR = trapezoidal). Table I summarizes these amplitudes for both modes A and B for sawtooth profile at 14.029 μm and 14.031 μm, and shows also the percentage difference of the amplitudes of other profiles with respect to the sawtooth D, as calculated at 14.029 μm. The alternating signs in some cases are due to the relevant coefficients of Fourier series expansion of grating profile.

In case of sinusoidal profile, the amplitudes of the real part of E_y field component of spurious harmonics for $n = 1$ (mode A) and (mode B) are dominant (in absolute value) with respect to the other harmonics, and are at least two orders of magnitude lower than the amplitudes of fundamental harmonics. In fact, when $n = 1$ (mode A) and (mode B), the equivalent permittivity assumes a minimum value because the sinusoidal profile admits only one spatial frequency, i.e., $\epsilon_o > 0$, $\epsilon_n = 0$, $n \neq 0$. Therefore, the guided spurious harmonics are weaker in the grating region for $n = 0$ than $n > 0$, giving stronger guiding, less coupling with the two slabs and much lower amplitudes with increasing n. In a similar way, the resonance condition (Λ = 14.031 μm) for sawtooth profile arises when the spurious harmonics in the grating region have minimum amplitudes. This can be seen in Table I by comparing the amplitudes for sawtooth profile calculated at 14.029 μm and 14.031 μm. Since the Fourier series expansion of sawtooth profile has its permittivity components in rigorously decreasing order, the space harmonic amplitudes are in decreasing order with increasing n, too (see Table I). Therefore, in Fig. 2 we observe that the curve for $n = -1$ (mode A) is closer to that for $n = 0$ (mode B) in case of sawtooth rather than for the sinusoidal profile, because the amplitudes of sawtooth spurious harmonics are smaller than those of the sinusoidal profile. In fact, the zeroth-order component $\epsilon_o(x)$ is larger in the sinusoidal than in the sawtooth profile, so contributing to a weaker guiding of the spurious harmonics in the grating region, a stronger coupling with the two slabs and larger amplitudes of spurious harmonics. In case of sawtooth profile, it can be noted from Table I that the amplitudes are globally (for both modes A and B) smaller than those for other profiles at the same period (14.029 μm). As a conclusion, the curves in Fig. 2 are explained by considering that the contribution of spurious harmonics to the total e.m. field is minimum at the resonance condition for sawtooth profile, while this contribution is increasingly greater for triangular, sinusoidal, trapezoidal and rectangular (50%) profile.

In particular, the rectangular profile exhibits a Fourier series expansion like a sinc(K) function, so giving both positive and negative not ordered components. This can be clearly seen from the amplitudes of space harmonics for mode A and mode

TABLE I
AMPLITUDES OF SPURIOUS HARMONICS FOR VARIOUS PROFILES

n	GADC with n_2=3.45, t = 0.1 μm			Mode A		
	(S)	(T)	(D) (14.029 μm)	(TR)	(Q)	(D) (14.031 μm)
1	+29.3%	+4.18%	0.01746	-99.5%	-266%	0.01726
2	-120.7%	-79.4%	0.006837	-60.1%	-41.1%	0.006738
3	-97.5%	-67.6%	0.003792	-33.6%	-248.6%	0.003732
4	-102.2%	-86%	0.002444	-75.5%	-33%	0.002403
5	-99.8%	-80.2%	0.001716	-99.6%	-244.2%	0.001687
6	-99.9%	-89%	0.001275	-86.8%	-29.9%	0.001253
7	-99.9%	-85.5%	0.0009857	-68.6%	-242.3%	0.0009682
8	-99.9%	-90.8%	0.0007847	-83.8%	-28.4%	0.0007706
9	-99.9%	-88.3%	0.0006387	-99.7%	-242.1%	0.0006271
				Mode B		
	(S)	(T)	(D)	(TR)	(Q)	(D)
2	-230.6%	-197.2%	0.06504	+64.7%	+111.6%	0.06086
3	-77.1%	-74.8%	0.02357	-65.5%	-147.8%	0.02211
4	-102.8%	-134.2%	0.01270	-152.9%	+104.2%	0.01195
5	-99.6%	-83.3%	0.008103	-99.9%	-155%	0.007624
6	-100.2%	-121.2%	0.005654	-64.5%	+99.3%	0.005322
7	-99.9%	-87.2%	0.004182	-88.3%	-158.1%	0.003938
8	-100.1%	-115.7%	0.003224	-125%	+96.8%	0.003037
9	-100%	-89.3%	0.002566	-99.9%	-161.2%	0.002417

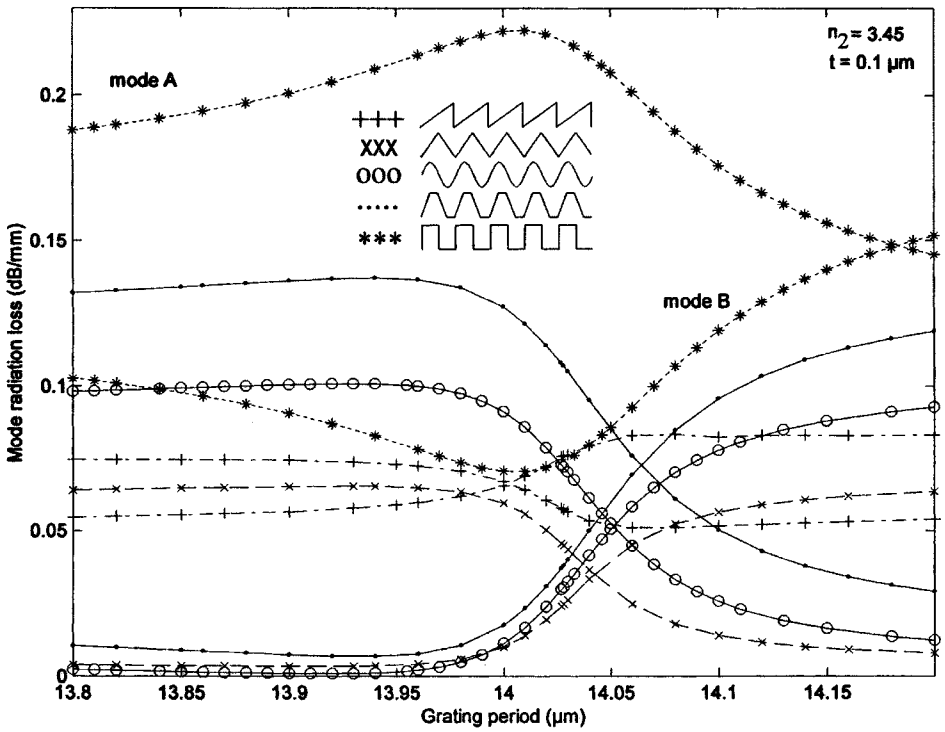

Fig. 3. Mode radiation loss (dB/mm) versus grating period for different index profiles, +++: sawtooth, ×××: symmetric triangular, ooo: sinusoidal, ...: symmetric trapezoidal, ***: squared (50%). GADC parameters: $n_o = 3.18$, $n_1 = 3.282$, $n_g = 3.18$, $n_r = n_{fr} = 3.282$, $n_2 = 3.45$, $n_s = 3.18$, $t_1 = 0.2$ μm, $t_r = 0.1$ μm, $t_g = 1.45$ μm, $t_{fr} = 0.45$ μm, $t_2 = 0.257$ μm.

B, as changed with respect to those of sawtooth profile (see Table I). Amplitudes larger than those occurring in sawtooth, sinusoidal, triangular or trapezoidal profile have been obtained. Therefore, the resonance condition occurs with a larger deviation wavenumber.

B. Mode Radiation Loss

The mode radiation loss depends strongly on the grating profile, as it can be seen in Fig. 3, where the radiation losses of both modes (A and B) are given versus the grating period for the index profiles above described.

The behavior of radiation loss curves can be explained by considering the amplitudes of radiating harmonics. For sawtooth profile, the amplitudes of radiating harmonics are in strictly decreasing order as those of spurious ones, then the harmonic $n = -1$ for mode B and $n = -2$ for mode A are dominant with respect to the others. In Fig. 4, the normalized radiation efficiency of space harmonics scattering in the substrate (S) and in the overlay (A) is sketched as a function of the grating period for the sawtooth profile. The normalization is referred to the net sum of all the radiation harmonics for each mode. It demonstrates that the dominant harmonics radiate the most of lost optical power in the substrate and in the overlay ($-1S$ and $-1A$ for $n = -1$, and $-2S$ and $-2A$ for $n = -2$, respectively), i.e., the space harmonics having propagation constant closer to guided harmonics radiate the most of optical power. Therefore, the curves of radiation loss for sawtooth profile (Fig. 3) follow the behavior of these dominant harmonics with changing the period. It must be noted that small values of period support the power scattering from lower to upper slab, while with large periods ($\Lambda > 14$ μm) the power scattering is favored in the opposite direction. This explains the decreasing (increasing) behavior of radiation loss for mode A (B). Moreover, the radiation loss of Fig. 3 is very small for both modes (sawtooth profile), even in the presence of a large number of harmonics ($N = 9$, i.e., 19 harmonics, have been considered). This is due to the fact that, as depicted in Fig. 4, the structure with sawtooth profile radiates power with changing the period in an orderly way, the $-2S$ space harmonic efficiency of mode A [$-2S(A)$] being always larger than $-2A$ and $-3S$, the efficiency of harmonic $-1S$ of mode B being larger than $-1A$ and $-2S$, and so on.

More symmetric profiles than sawtooth, as triangular or sinusoidal, also exhibit losses quite low, but an increasing contribution to total loss of the mode A with respect to B occurs, since the dominant radiating harmonic of mode A ($n = -2$, see Fig. 5 for triangular profile) scatters more power (compare with Fig. 4). It is immediate to think that index profiles described by a larger number of harmonics presents an increasing radiation effect, as confirmed by the curves relevant to the rectangular (50%) profile (***) in Fig. 3. Here, the losses of both modes are larger than in other profiles, since a significant power is radiated by a number of space harmonics, ranging from $n = -2$ to -9 (mode A) and from to -9 (mode B). The curves of radiation losses are characterized by an increasing (decreasing) and then decreasing (increasing) behavior for mode A (B), as it is clear in the curves of rectangular profile and, more slightly, in the others. This behavior can be understood from Fig. 6, where the normalized radiation efficiency is reported as a function of

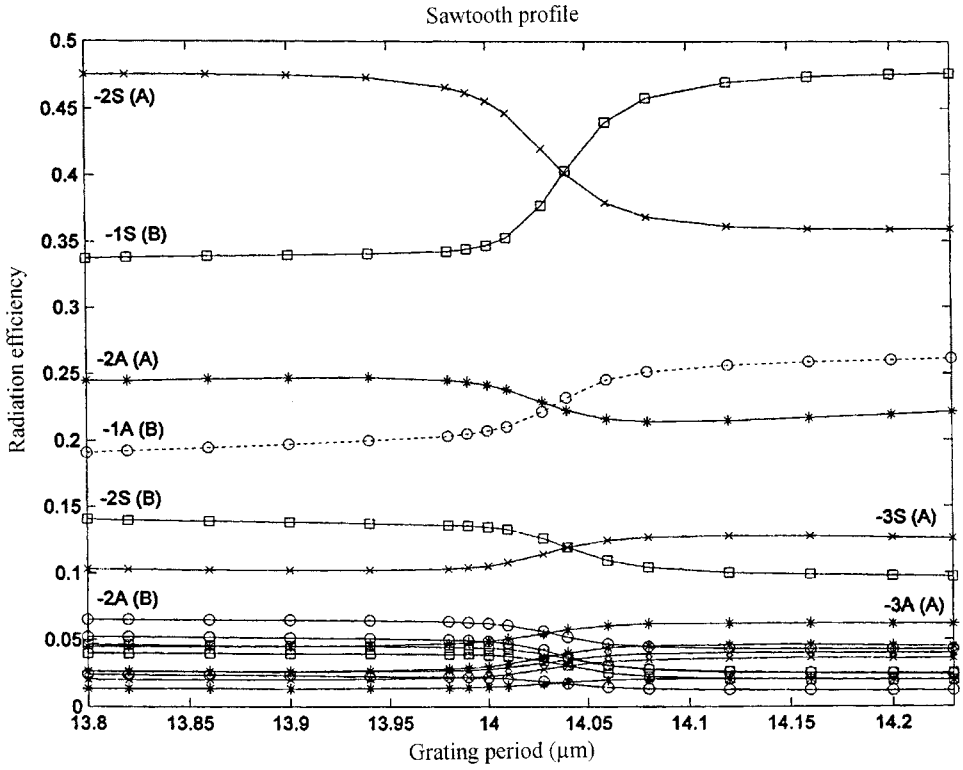

Fig. 4. Normalized radiation efficiency of space harmonics in the overlay (A) and substrate (S) versus grating period for sawtooth profile (modes A and B).

the grating period. A comparison of curves in Fig. 6 with those in Fig. 3 clearly shows that $-1S$ constitutes the dominant space harmonic of the mode B. By similar considerations, the curve of radiation loss for mode A mainly depends on $-2A$ space harmonic, which is dominant too. Then, the strong increase of mode radiation loss (Fig. 3) for the rectangular profile with respect to other profiles (in particular, sawtooth) is connected to larger radiation efficiency of dominant harmonics and larger number of harmonics radiating significant power at each grating period (i.e., stronger power mixing among the higher order harmonics).

Results for sinusoidal profile demonstrate that the small loss decrease for mode B (see Fig. 3) is due to the behavior of -1 harmonic radiating in the substrate $(-1S)$, which strongly decreases up to $\Lambda = 13.95$ μm, and then increases. Since the behavior of -1 harmonic radiating in the overlay $(-1A)$ is absolutely symmetric, the radiation loss curve demonstrates that $n = -1$ radiating in the substrate again constitutes the dominant space harmonic for mode B and, similarly, the curve of radiation loss for mode A depends on $-2A$ space harmonic. The curves of radiating efficiency for triangular profile (Fig. 5) confirm that the dominant harmonic is $-1S$ for mode B and $-2A$ for mode A. This profile has intermediate characteristics between sawtooth and rectangular both for shape, coefficients of Fourier series expansion and harmonic amplitudes, and the distribution of radiation efficiency presents intermediate properties, too. In fact, the radiated power mixing among the harmonics increases from sawtooth to triangular to rectangular profile.

C. Coupling Length and Efficiency

The electric field y-component for the modes A (ϕ_A, including the $n = -1$ and "0" space harmonics) and B (ϕ_B, with $n = 0$ and $+1$) have been calculated at the resonance for a number of profiles, i.e., sinusoidal, sawtooth, rectangular and triangular. For example, in case of sinusoidal profile it is clear that the overlapping of these field distributions $(\phi_A + \phi_B)$ produces the field reinforcement in the upper slab and the field reduction in the lower guide (first case). The contrary occurs in the second case, when $(\phi_A - \phi_B)$.

Since each guided mode is given by only two space harmonics, we can write

$$\begin{aligned}\phi_A(x) &\approx [f_0^A(x) + f_{-1}^A(x)e^{-jKz}]\exp[j(\beta_0^A + j\alpha_A)z]\\ \phi_B(x) &\approx [f_0^B(x) + f_{+1}^B(x)e^{jKz}]\exp[j(\beta_0^B + j\alpha_B)z]\end{aligned} \quad (13)$$

and the total EM-field is

$$\begin{aligned}&|\phi_A(x) \pm \phi_B(x)|\\ &\quad\approx |e^{j\beta_0^A}[f_0^A(x)e^{-\alpha_A z} + f_{-1}^A(x)e^{-\alpha_A z}e^{-jKz}]\\ &\qquad \pm e^{j\beta_0^B}[f_0^B(x)e^{-\alpha_B z} + f_1^B(x)e^{-\alpha_B z}e^{jKz}]|\end{aligned} \quad (14)$$

where α_A, α_B are the relevant leakage factors. Since $\beta_0^B = \beta_0^A - K - \delta$, (14) can be rearranged in the form

$$\begin{aligned}&|\phi_A(x) \pm \phi_B(x)|\\ &\quad\approx |f_0^A(x)e^{-\alpha_A z} + f_{-1}^A(x)e^{-\alpha_A z}e^{-jKz}\\ &\qquad \pm f_0^B(x)e^{-\alpha_B z}e^{-jKz}e^{-j\delta z}\\ &\qquad \pm f_1^B(x)e^{-\alpha_B z}e^{-j\delta z}|.\end{aligned} \quad (15)$$

In $z = 0$, we have

$$\begin{aligned}|\phi_A(x) \pm \phi_B(x)| \approx |&f_0^A(x) + f_{-1}^A(x)\\ &\pm f_0^B(x) \pm f_1^B(x)|.\end{aligned} \quad (16)$$

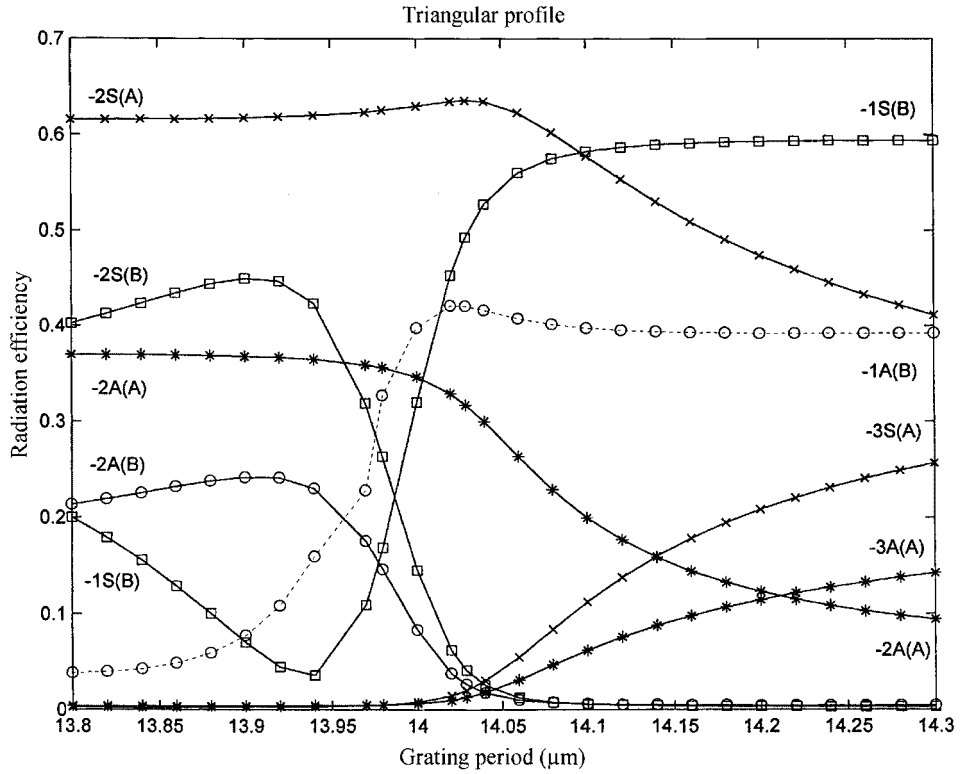

Fig. 5. Normalized radiation efficiency of space harmonics in the overlay (A) and substrate (S) versus grating period for triangular profile (modes A and B).

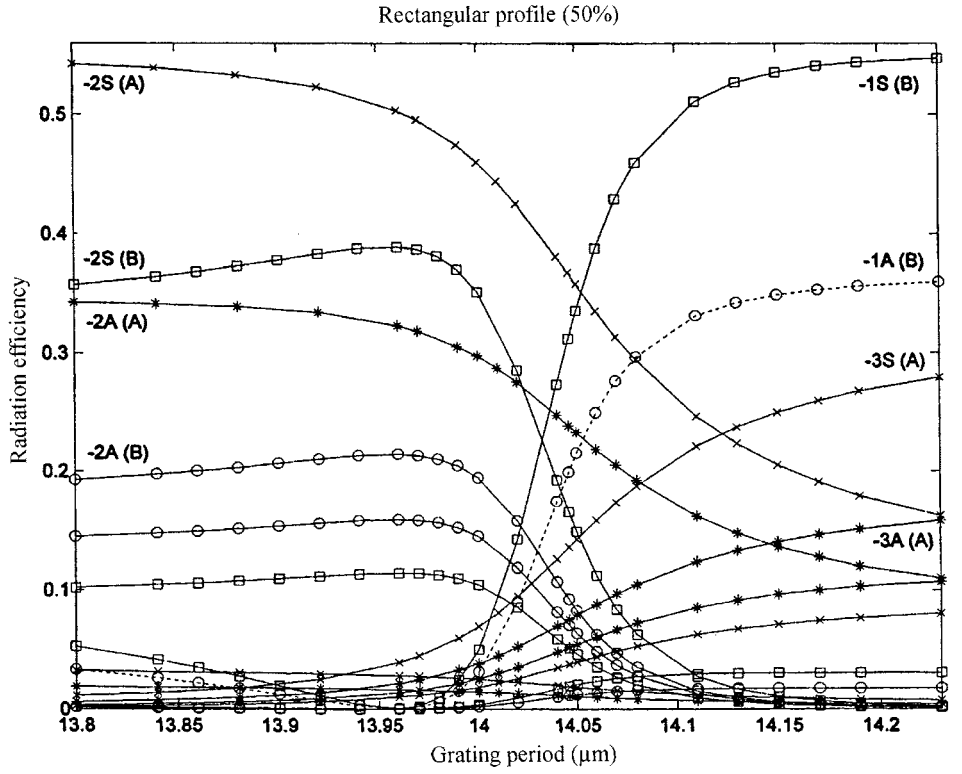

Fig. 6. Normalized radiation efficiency of space harmonics in the overlay (A) and substrate (S) versus grating period for rectangular (50%) profile (modes A and B).

In other words, the EM-field is given by two contributions in both cases [sign $+$ or $-$ in (14)–(16)], the former depending on the couple (f_0^A, f_1^B) and the latter on the couple (f_{-1}^A, f_0^B) of quasi-synchronous components, respectively. By minimizing

one contribution with respect to the other, the condition of maximum power transfer (coupling length, L_c) in both cases can be found by (17) at the bottom of the page.

The coupling efficiency in both cases is given by (18) also shown at the bottom of the page.

D. Influence of Lower Slab Refraction Index

A detailed investigation of Marcuse structure [8] as a function of lower slab refraction index has been carried out. First, the resonance condition has been determined at $t = 0.1$ μm, $n_2 = 3.282$, for sinusoidal and rectangular (50%) profiles. Results give $\Lambda = 26.775$ μm (sinusoidal) and $\Lambda = 26.799$ μm (rectangular). Then, the coupling length and efficiency have been determined by (17) and (18) for rectangular profile at $\Lambda = 26.775$ and $\Lambda = 26.799$ μm. The values show a very little difference (-0.088%), i.e., $L_c = 1.4726$ mm and 1.4739 mm, respectively, which is shorter than one grating period. A slightly greater difference (-0.97%) has been obtained at $n_2 = 3.45$, $t = 0.1$ μm, i.e., $L_c = 1.4730$ mm ($\Lambda = 14.029$ μm) and 1.4875 mm ($\Lambda = 14.033$ μm), which is of the order of one grating period and, then, negligible. In this last case, the efficiency results 98%. This circumstance demonstrates that the resonance condition obtained by sinusoidal profile represents a very good, practical approximation of grating period, even for strongly asymmetric GADC's. Since only five space harmonics ($N = 2$) are to be used in the calculations with sinusoidal profile instead of a minimum of 19 ($N = 9$) for more complicated profiles (such as sawtooth, rectangular or triangular), the required average CPU time is much lower (3 s instead of 85 s by using a 233-MHz compatible PC). This allows a very fast procedure for real time optimal design of arbitrary GADC structures, since the search of resonance condition is the more critical aspect.

The resonance periods (Λ) have been calculated by sinusoidal profile in a number of cases, ranging from $n_2 = 3.282$ to $n_2 = 3.52$, together with the grating period (Λ_o), approximated by CMT. The percentage error is less than 0.07%. It is interesting to note that the optimal period increases with increasing n_2 for moderate asymmetric structures (having $n_2 < 3.3$), while it decreases for strongly asymmetric ones. A significant discrepancy (-0.12%) in the evaluation of resonance condition has been observed with respect to results given in [15] for $n_2 = 3.45$. This is probably due to the limited number (12) of space harmonics retained in that algorithm, while in this work 19 space harmonics radiating in the overlay and 19 in the substrate have been used. The coupling lengths and coupling efficiency, as calculated by (17) and (18), are shown in Figs. 7 and 8, respectively, for different grating profiles (solid lines). An optimal rectangular profile, with optimized duty cycle has been also determined by reducing the coupling length as much as possible. The minimum coupling length is obtained with a duty cycle ranging from 42% (for $n_2 = 3.282$) to 32% (for $n_2 = 3.52$). In Fig. 7, the increase of coupling length for $n_2 > 3.47$ obtained with a lower duty cycle (29%) is also shown for comparison. Coupling lengths calculated for $n_2 > 3.42$ are practically the same if the duty cycle is included between 32% and 50%, but at the expenses of a lower coupling efficiency (see Fig. 8). Therefore, the "inf" and "sup" section lengths of the grating period are demonstrated to be not critical parameters even for strongly asymmetric GADC. In Fig. 7 the coupling length as calculated by Marcuse [8] is also given, showing that results derived by CMT and similar methods are usually underestimated. Our results demonstrate that the coupling length increases versus the index profile as closer as the effective index of mode A with respect to that of mode B (see Fig. 2), as expected. In other words, the sawtooth profile represents the worst case with respect to the coupling length and the best to the radiation loss, while the contrary occurs for rectangular profile.

The curves of coupling efficiency (Fig. 8) show a strong dependence of asymmetric profiles on the degree of GADC asymmetry, while a slight dependence of symmetric profiles, such as sinusoidal, triangular and rectangular (50%) can be noted. This circumstance occurs because the symmetric profiles scatter the radiated power by higher order space harmonics toward the sub-

$$\varphi(L_c) = \min[\varphi(z)] \tag{17}$$

where

$$\varphi(z) = \left| \frac{\cos(\delta z/2) \displaystyle\int_{-\infty}^{+\infty} [f_0^A(x) e^{-\alpha_A z} \pm f_1^B e^{-\alpha_B z}]\, dx + j \sin(\delta z/2) \int_{-\infty}^{+\infty} [f_0^A(x) e^{-\alpha_A z} \mp f_1^B e^{-\alpha_B z}]\, dx}{\cos(\delta z/2) \displaystyle\int_{-\infty}^{+\infty} [f_{-1}^A(x) e^{-\alpha_A z} \pm f_0^B e^{-\alpha_B z}]\, dx + j \sin(\delta z/2) \int_{-\infty}^{+\infty} [f_{-1}^A(x) e^{-\alpha_A z} \mp f_0^B e^{-\alpha_B z}]\, dx} \right|.$$

$$\eta = \frac{\displaystyle\int_{-\infty}^{+\infty} |\cos(\delta z/2)\, [f_{-1}^A(x) e^{-\alpha_A L_c} \pm f_0^B e^{-\alpha_B L_c}] + j \sin(\delta z/2)\, [f_{-1}^A(x) e^{-\alpha_A L_c} \mp f_0^B e^{-\alpha_B L_c}]|^2\, dx}{\displaystyle\int_{-\infty}^{+\infty} |f_{-1}^A(x) \mp f_0^B|^2\, dx}. \tag{18}$$

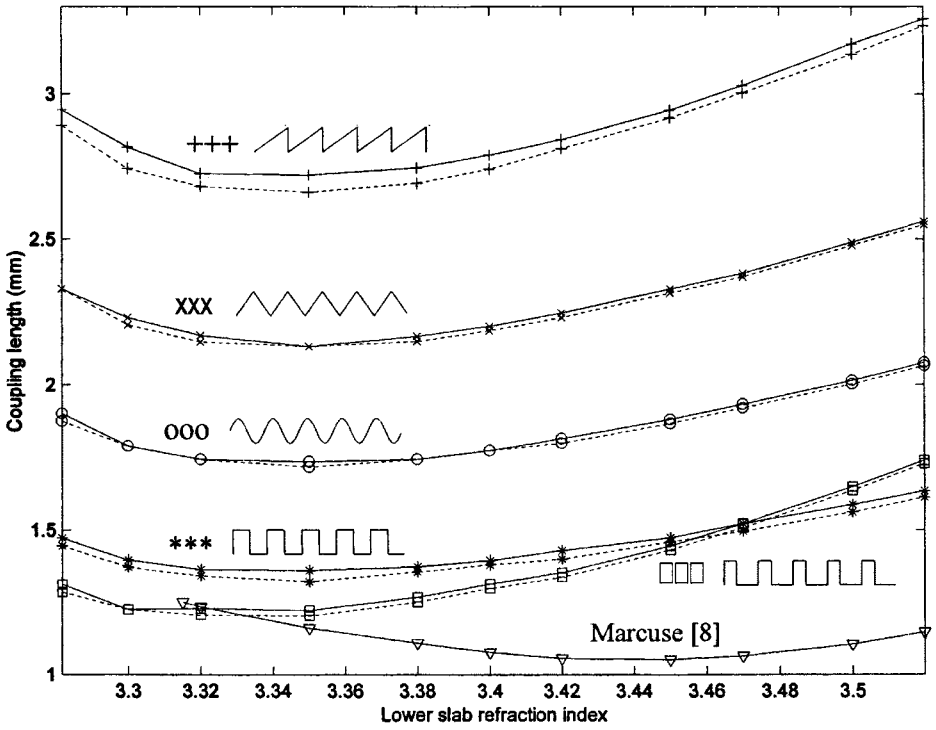

Fig. 7. Coupling length (mm) versus lower slab refraction index n_2 for different index profiles, +++: sawtooth, $\times\times\times$: symmetric triangular, ooo: sinusoidal, ***: squared (50%), boxes: optimized rectangular (duty cycle ranging from 42% to 32%). GADC parameters: $n_o = 3.18, n_1 = 3.282, n_g = 3.18, n_r = n_{fr} = 3.282, n_s = 3.18, t_1 = 0.2\ \mu$m, $t_r = 0.1\ \mu$m, $t_g = 1.45\ \mu$m, $t_{fr} = 045\ \mu$m, t_2 ranging from 0.4238 to 0.2280 μm. This paper (solid line) and [16] (dashed line). The predictions by Marcuse [8] are also shown.

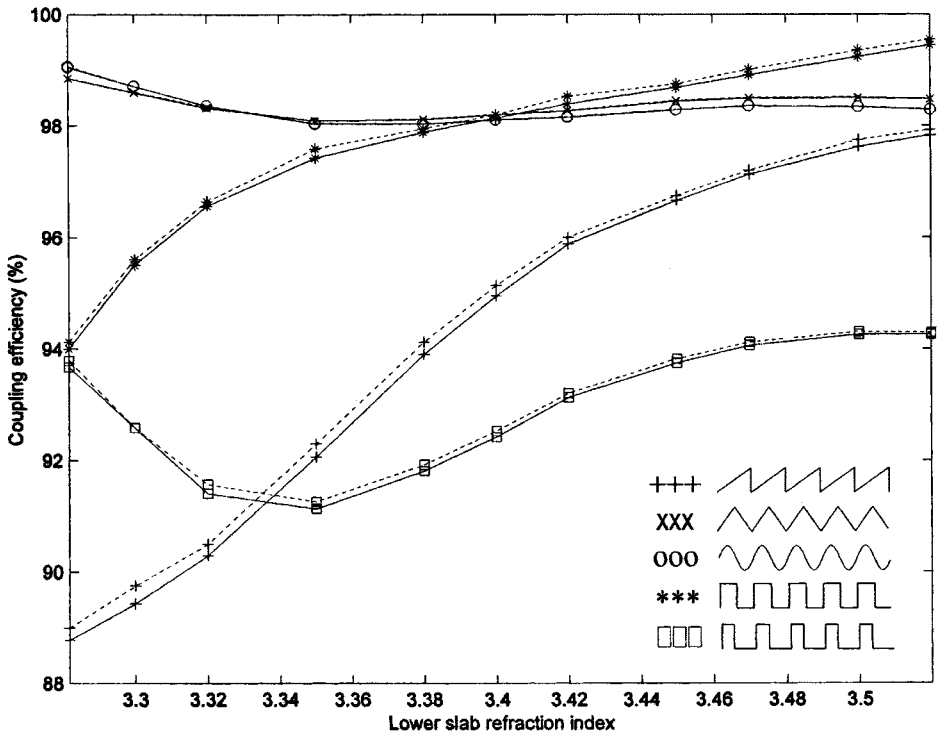

Fig. 8. Coupling efficiency (%) versus lower slab refraction index n_2 for different index profiles, +++: sawtooth, xxx: symmetric triangular, ooo: sinusoidal, ***: squared (50%), boxes: optimized rectangular (duty cycle ranging from 42 to 32%). GADC parameters: $n_o = 3.18, n_1 = 3.282, n_g = 3.18, n_r = n_{fr} = 3.282, n_s = 3.18, t_1 = 0.2\ \mu$m, $t_r = 0.1\ \mu$m, $t_g = 1.45\ \mu$m, $t_{fr} = 0.45\ \mu$m, t_2 ranging from 0.4238 to 0.2280 μm. This paper (solid line) and [16] (dashed line).

strate and overlay in a similar way, less influenced by the index difference between the two GADC slabs. On the contrary, asymmetric profiles such as sawtooth and rectangular ones exhibit a different scattering in the substrate and the overlay, depending on the GADC structure, and the coupling efficiency varies a lot. Therefore, a smaller coupling length must be paid by a lower

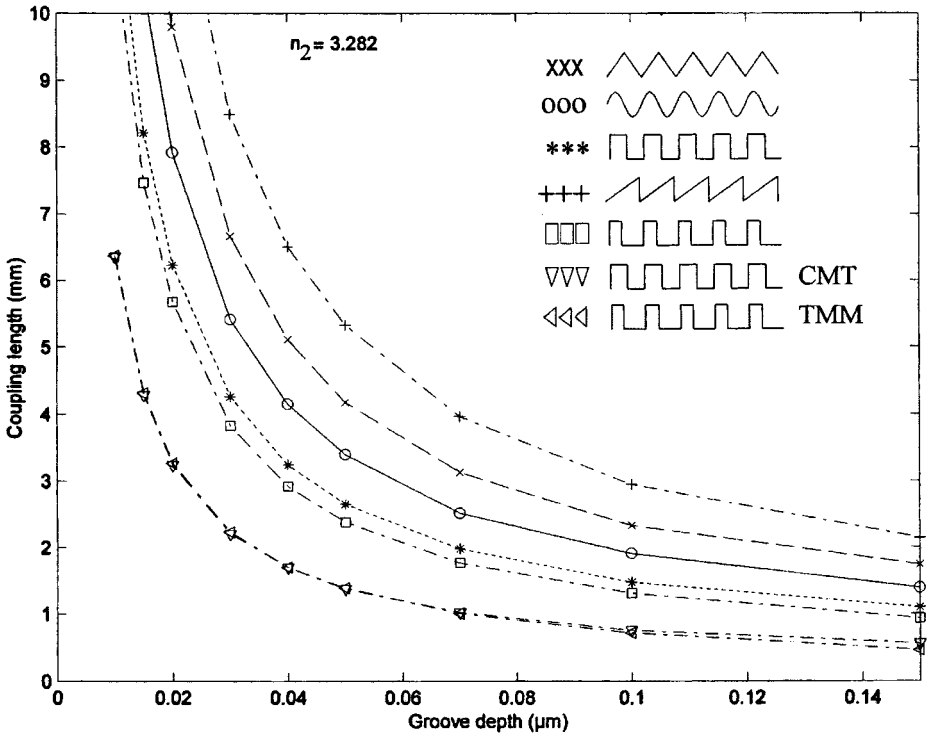

Fig. 9. Coupling length (mm) versus grating depth (μm) for different index profiles, +++: sawtooth, $\times\times\times$: symmetric triangular, ooo: sinusoidal, ***: squared (50%), boxes: optimized rectangular (42%). GADC parameters: $n_o = 3.18$, $n_1 = 3.282$, $n_g = 3.18$, $n_r = n_{fr} = 3.282$, $n_s = 3.18$, $t_1 = 0.2$ μm, $t_2 = 0.4238$ μm, $t_g = 1.5 - t_r/2$ μm, $t_{fr} = 0.5 - t_r/2$ μm, t_r ranging from 0.01 to 0.15 μm. CMT and TMM predictions are included.

coupling efficiency. Results have been compared with those calculated by (12) and by the following approximated expression given in [16]:

$$\tan\left(\frac{\delta L_c}{2}\right) = \frac{\delta}{2\alpha}. \tag{19}$$

The agreement of our results with those obtained by (12) is very good, the error being less than 2.4%, while (19) leads to more approximated values, with an error of about 4.9%. Fig. 7 shows the predictions by (19) as dashed lines, while in Fig. 8 the relevant coupling efficiencies are sketched. This is because the mode radiation losses are not usually negligible and, in particular, are not equal (particularly in rectangular profiles), as assumed in [16]. Therefore, the LMP approach, derived by Floquet theory, is confirmed to be an extension of the coupled mode theory involving leaky modes and an arbitrary number of higher order space harmonics, where the (12) can be again used with the values of propagation constants corrected by the presence of the grating. This is a general result, not depending on the GADC parameters, such as lower slab refraction index or groove depth, or grating profile.

E. Influence of Grating Depth

Calculations of coupling length and efficiency have been also performed as a function of groove depth. Figs. 9 and 10 show the coupling length and efficiency obtained for different grating profiles at $n_2 = 3.282$ (quasi-symmetric GADC), with t ranging from 0.01 to 0.15 μm. The curves have been determined by evaluating the resonance condition versus the groove depth by using the sinusoidal profile. The symmetric profiles exhibit higher efficiency with respect to the asymmetric ones with increasing the groove depth, but the best condition (lowest coupling length) is obtained again with the optimized rectangular profile (42%), which is characterized by a larger value of δ. In our calculations the resonance condition has been compared with that predicted by CMT and TMM approaches with changing t, the maximum difference being -0.067% (CMT) and $+0.73\%$ (TMM) at $t = 0.15$ μm. Then, the coupling length and efficiency have been calculated by the three methods (LMP, CMT, and TMM). The aim was to establish how critical is the evaluation of grating period and its influence on the predictions of coupling length and efficiency, even in GADC with moderate asymmetry. It is clear that an increasing discrepancy of LMP results from those obtained by more approximated methods can be noted as large as the groove depth. Predictions of coupling length by CMT (-42.25%) and TMM (-45.45%) at $t = 0.1$ μm are strongly underestimated, also for very small groove depths. Moreover, the coupling efficiency as calculated by both CMT and TMM is much lower than that in Fig. 10, of the order of 60%.

Finally, an investigation of the influence of the grating period on the coupling efficiency has been carried out for the GADC structure with $n_2 = 3.45$ and $t = 0.1$ μm. Results demonstrate that the fabrication tolerance is greater for rectangular (about 0.2 μm, with efficiency changing from 98% to 60% and duty cycle from 33 to 50%) than for sinusoidal profile (about 0.16

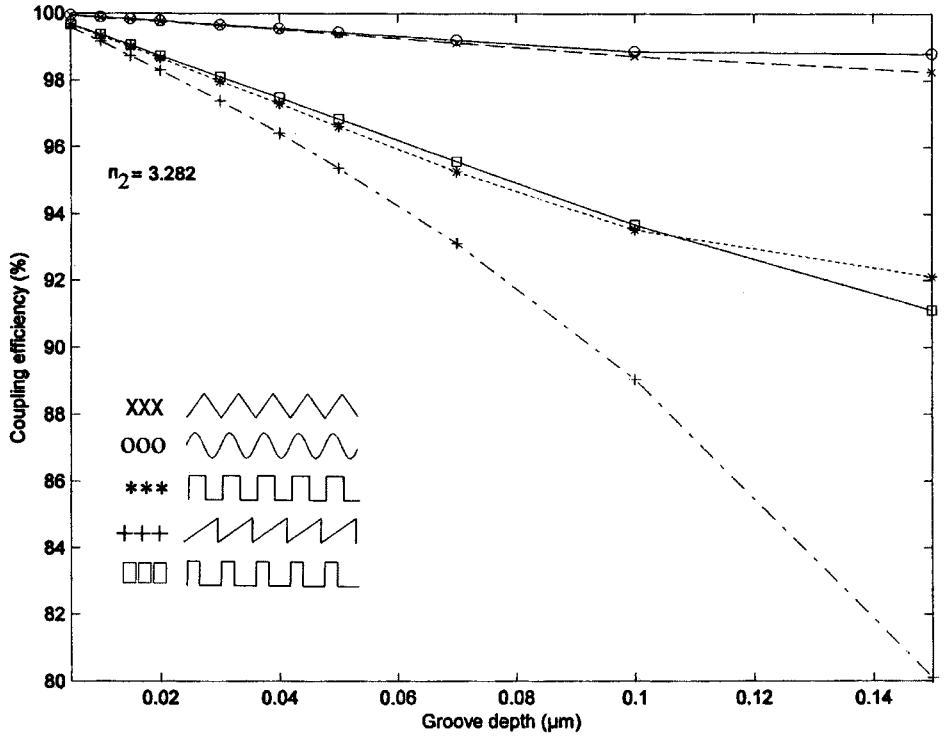

Fig. 10. Coupling efficiency (%) versus grating depth (μm) for different index profiles, +++: sawtooth, $\times\times\times$: symmetric triangular, ooo: sinusoidal, ***: squared (50%), boxes: optimized rectangular (42%). GADC parameters: $n_o = 3.18$, $n_1 = 3.282$, $n_g = 3.18$, $n_r = n_{fr} = 3.282$, $n_s = 3.18$, $t_1 = 0.2$ μm, $t_2 = 0.4238$ μm, $t_g = 1.5 - t_r/2$ μm, $t_{fr} = 0.5 - t_r/2$ μm, t_r ranging from 0.01 to 0.15 μm.

μm), since the former is less influenced by the period changes around the resonance condition.

IV. Conclusion

The rigorous approach of leaky mode propagation has been used for the optimal design of InP–InGaAsP–InP–InGaAsP–InP grating-assisted directional couplers. A detailed explanation of GADC behavior versus index profile is given, showing that the minimum wavenumber deviation is obtained in asymmetric GADC with strongly asymmetric profiles, as sawtooth. Calculations of grating period, radiation loss, coupling length and efficiency demonstrate that the LMP approach can be seen as an extension of CMT even for GADC with high index asymmetry. In particular, the sinusoidal profile, whose resonance condition can be obtained by using a very low number of harmonics ($N = 2$), allows to design GADC structures in real time, since the resonance condition of any GADC having arbitrary profile can be evaluated with high accuracy (error less than 0.03%) and very short CPU average time (3 s instead of 85 s for the rectangular profile with $N = 9$, by using a 233-MHz compatible PC). The rectangular profile is demonstrated to be the best choice for minimizing the coupling length at the expenses of a large radiation loss and reduced coupling efficiency, if an appropriate duty cycle is used. Larger coupling efficiency and smaller radiation loss can be achieved by strongly asymmetric profiles as sawtooth, but with much larger lengths. Results of coupling length and efficiency have been also obtained and compared with alternative techniques, i.e., CMT and TMM, for GADC having moderate thickness asymmetry. Increasing discrepancies have been found in the calculations by LMP with respect to TMM and CMT as large as the grating depth. As a conclusion, the rigorous LMP method has allowed to determine how critical is the grating period on the GADC design parameters and performance. Further investigations will be possible by this method for studying the wavelength dependence (spectral behavior) of strongly asymmetric structures as a function of grating depth.

Acknowledgment

The author wishes to thank Prof. M. N. Armenise for his suggestions, comments, and critical reading of the paper. He would also like to thank the referees for their comments and suggestions.

References

[1] B. Little and T. Murphy, "Design rules for maximally flat wavelength-insensitive optical power dividers using Mach-Zehnder structures," *IEEE Photon. Technol. Lett.*, vol. 9, no. 12, pp. 1607–1609, 1997.

[2] S. Oku, S. Kondo, Y. Noguchi, T. Hirono, M. Nakao, and T. Tamamura, "Fabrication and performance of InGaAlAs MQW distributed Bragg reflector lasers with grooved surface gratings formed by reactive beam etching," *Inst. Elect. Eng. Proc. Pt. J*, vol. 146, no. 1, pp. 39–43, 1999.

[3] D. Weismann, D. Erni, J. Frohlich, H. Rothuizen, R. Germann, G.-L. Bona, C. David, and H. Jackel, "Apodization of a grating filter by concatenation of Bragg gratings with different ridge patterns," in *Proc. IX Eur. Conf. Int. Optics (ECIO'99)*, 1999, pp. 159–162.

[4] L. L. Buhl, R. C. Alferness, U. Koren, B. I. Miller, M. G. Young, T. L. Koch, C. A. Burrus, and G. Raybon, "Grating assisted vertical coupler/filter for extended tuning range," *Electron. Lett.*, vol. 29, no. 1, pp. 81–82, 1993.

[5] T. L. Koch, P. J. Corvini, W. T. Tsang, U. Koren, and B. I. Miller, "Wavelength selective interlayer directionally grating-coupled InP/InGaAsP waveguide photodetection," *Appl. Phys. Lett.*, vol. 51, no. 14, pp. 1060–1062, 1987.

[6] D. Marcuse, "Directional couplers made of nonidentical asymmetric slabs. Part II: Grating-assisted couplers," *J. Lightwave Technol.*, vol. LT-5, no. 2, pp. 268–273, 1987.
[7] W. P. Huang, J. Hong, and Z. M. Mao, "Improved coupled-mode formulation based on composite modes for parallel grating-assisted co-directional couplers," *IEEE J. Quantum Electron.*, vol. 29, no. 11, pp. 2805–2812, 1993.
[8] D. Marcuse, "Radiation loss of grating-assisted directional coupler," *IEEE J. Quantum Electron.*, pp. 675–684, 1990.
[9] S. Srivastava, N. Gupta, M. Saini, and E. K. Sharma, "Power exchange in coupled optical waveguides," *J. Opt. Commun.*, vol. 18, no. 1, pp. 5–9, 1997.
[10] B. E. Little, "Junction problem and loading effects in grating-assisted couplers," *Opt. Lett.*, vol. 21, no. 13, pp. 949–951, 1996.
[11] ——, "A variational coupled-mode theory including radiation loss for grating-assisted couplers," *J. Lightwave Technol.*, vol. 14, pp. 188–195, Feb. 1996.
[12] W. Huang and J. Hong, "Transfer matrix approach based on local normal modes for coupled waveguides with periodic perturbations," *J. Lightwave Technol.*, vol. 10, pp. 1367–1375, Oct. 1992.
[13] K. C. Chang, V. Shah, and T. Tamir, "Scattering and guiding of waves by dielectric gratings with arbitrary profiles," *J. Opt. Soc. Amer.*, vol. 70, no. 7, pp. 804–813, 1980.
[14] V. M. N. Passaro and M. N. Armenise, "Analysis of radiation loss in grating-assisted codirectional couplers," *IEEE J. Quantum Electron.*, vol. 31, pp. 1691–1697, Sept. 1995.
[15] N.-H. Sun, J. K. Butler, G. A. Evans, L. Pang, and P. Congdon, "Analysis of grating-assisted directional couplers using the floquest-bloch theory," *J. Lightwave Technol.*, vol. 15, pp. 2301–2314, 1997.
[16] J. K. Butler, N.-H. Sun, G. A. Evans, L. Pang, and P. Congdon, "Grating-assisted coupling of light between semiconductor and glass waveguides," *J. Lightwave Technol.*, vol. 16, pp. 1038–1048, 1998.
[17] N. Finger and E. Gornik, "Analysis of metallized-grating coupled twin-waveguide structures," *IEEE J. Quantum Electron.*, vol. 35, pp. 832–843, 1999.
[18] D. Marcuse, "Directional couplers made of nonidentical asymmetric slabs. Part I: Synchronous couplers," *J. Lightwave Technol.*, vol. LT-5, pp. 113–118, 1987.

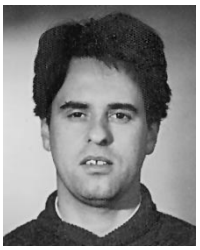

Vittorio M. N. Passaro (M'92) was born in Bari, Italy, in November 1962. He received the laurea degree in electronic engineering from the University of Bari, Italy, in 1988 and the Ph.D. degree in electronic engineering from the Polytechnic of Bari, Italy, in 1992.

He joined the Polytechnic of Bari as a Researcher of Electronics in 1991. Since 1988, his principal research interests have been in the fields of optoelectronics and integrated optics. His interests include fabrication and characterization techniques of lithium niobate-based optical waveguides and devices, and design and simulation of guided-wave devices and circuits in ferroelectric and semiconductor materials for optical signal processing, optical computing and optical control of microwaves. He is the author or coauthor of more than 50 journal articles and conference presentations.

Dr. Passaro is a member of SPIE, AEI (Associazione Elettrotecnica Italiana), and SIOF (Societa' Italiana di Ottica e Fotonica).